ARTICLE IN PRESS

Available online at www.sciencedirect.com
SCIENCE DIRECT®

Physics of the Earth and Planetary Interiors xxx (2004) xxx–xxx

PHYSICS OF THE EARTH AND PLANETARY INTERIORS

www.elsevier.com/locate/pepi

Superplumes or plume clusters?

G. Schubert [a,*], G. Masters [b], P. Olson [c], P. Tackley [a]

[a] *Department of Earth and Space Sciences, Institute of Geophysics and Planetary Physics, University of California, Los Angeles, CA, USA*
[b] *Institute of Geophysics and Planetary Physics, University of California, San Diego, USA*
[c] *Department of Earth and Planetary Sciences, The Johns Hopkins University, USA*

Received 28 February 2003; accepted 23 September 2003

Abstract

It is proposed that the broad, seismically slow, mantle structures under Africa and the Pacific, often identified as superplumes, are instead spatial clusters of smaller plumes. Seismic data, including ScS-S differential travel time residuals and tomographic inversions using ScS-S and deep turning S data, show the breakup of so-called superplume regions into smaller structures. For example, the superplume under Africa is clearly formed by at least two and possibly three distinct plumes while the superplume under the Pacific consists of at least six smaller plumes. Enhanced seismic resolution may reveal even smaller-scale structures in the superplume regions. Dynamical considerations argue for the plausibility of superplume regions being clusters of smaller plumes whose heads might have merged into a large region of hot and buoyant material. Alternatively, the superplumes may simply be large, passively upwelling regions that are seismically distinct.

Keywords: Mantle plumes; Mantle convection; Superplumes

1. Introduction

Seismic tomography (Su et al., 1994; Masters et al., 1996; Ritsema et al., 1999; Mégnin and Romanowicz, 2000) has revealed the existence of two broad (10,000 km across), seismically slow regions in the lower mantle that some have identified as superplumes. The locations of these regions, under the south-central Pacific and under Africa, correlate to the positions of two major geoid highs and to concentrations of hotspots (Hager et al., 1985). Zones of high seismic attenuation in the upper mantle lie vertically above the lower mantle low-velocity regions suggesting the existence of low-velocity structures or superplumes that extend continuously throughout the mantle from the core-mantle boundary to the lithosphere (Romanowicz and Gung, 2002) Are these regions really superplumes? Assuming that they are also hot, they are probably regions of broad mantle upwelling (Forte and Mitrovica, 2001), but does that make them superplumes? What is a superplume anyway?

In this paper we explore the idea that the resolution of previous seismic inversions is not adequate to reveal the smaller-scale structure of these regions. We present new seismic data showing the breakup of these regions in the lower mantle into at least several smaller plumes that may in turn consist of even

* Corresponding author. Tel.: +1-310-825-4577; fax: +1-310-825-2779.
E-mail addresses: schubert@ucla.edu (G. Schubert), guy@mahi.ucsd.edu (G. Masters), olson@jhu.edu (P. Olson), ptackley@ess.ucla.edu (P. Tackley).

0031-9201/$ – see front matter © 2004 Elsevier B.V. All rights reserved.
doi:10.1016/j.pepi.2003.09.025

smaller structures yet invisible to the seismic eye. We use dynamical considerations to argue that the regions are clusters of smaller structures or plumes that originate at the core-mantle boundary (CMB) and perhaps merge into a more or less continuous agglomeration of plume heads at some distance above the CMB.

2. Seismic evidence of structure within superplumes

Superplumes have been robust features of global tomographic models for well over a decade (e.g., Su et al., 1994; Masters et al., 1996). These early models were typically parameterized in spherical harmonics truncated at degree 12 or 16 and convincingly imaged large regions of low S velocity in the lower mantle under Africa and the Pacific. The question of whether these regions were really made up of a cluster of smaller low-velocity regions could not be addressed with the data then available. Beginning in about 1994, a rapid expansion of the global seismic network has now resulted in sufficiently improved coverage that we can begin to address the question of fine-scale structure.

The inversions described here are whole mantle inversions which incorporate large datasets of differential travel times (14,000 ScS-S measurements, 28,000 SS-S measurements), 70,000 direct S measurements, and Love and Rayleigh wave phase velocity data spanning the frequency range 4–15 mHz. In addition to these data, we also include new datasets of SS and S measurements made using an algorithm which clusters seismic traces based on their similarity and measures differential travel times between them. This algorithm allows us to efficiently process data and has resulted in over 120,000 S times at teleseismic distances. The inversion follows the method described by Masters et al. (2000) and uses a simple parameterization of equal area blocks of dimension 4° at the equator and with a thickness of 200 km in the lower mantle. This block dimension is about twice the wavelength of shear waves at the base of the mantle.

Despite the comprehensive nature of our dataset, the geometry of sources and receivers means that there are regions of poor coverage near the base of the mantle. As an example, we plot the differential travel times of ScS-S binned by the geographic bounce point of the ScS phase (Fig. 1). For this particular dataset, the geometry of sources and receivers means that there are two poorly sampled regions both of which are close to the superplume areas. The “hole” under the Pacific is largely filled by the dataset of direct turning S but the southern Indian Ocean remains poorly sampled. Despite coverage problems, Fig. 1 does indicate quite a lot of structure in the superplume region in the western Pacific and it is clear that there are two and possibly three distinct slow regions under Africa.

Fig. 2 shows the result of formal inversion for S velocity perturbation. We plot only the four lowermost

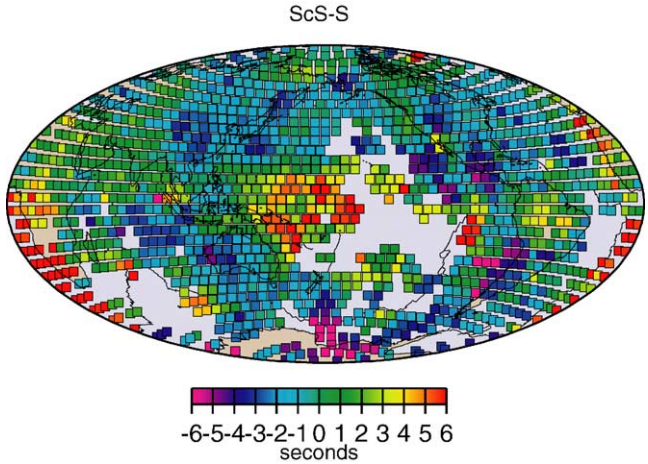

Fig. 1. ScS-S differential travel time residuals binned at the bounce point of the ScS phase on the CMB. The color scale is in seconds.

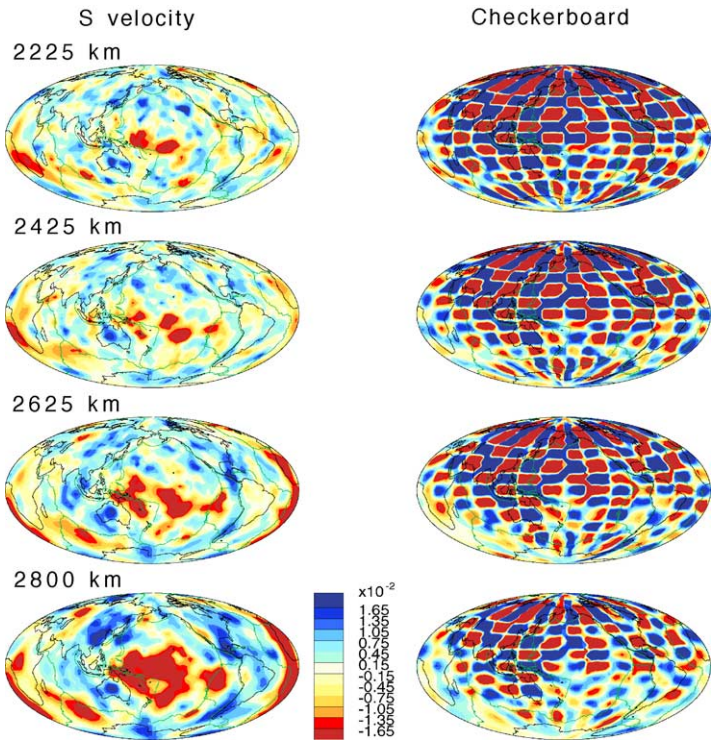

Fig. 2. Left column: Shear velocity in the four lowermost layers of a whole mantle model obtained by inverting the datasets described in the text. Perturbations about a mean 1D model are shown and are in excess of 2% at the base of the mantle. Right column: Checkerboard tests for each of the four layers. The reduced resolution in the southern hemisphere of the lowermost mantle implies that our model is too smooth and too low in amplitude there. Resolution is much improved in the layers above.

layers of the mantle (left side). On the right is the result of a checkerboard test for each of the layers. The grid size of the checkerboard is chosen to be similar to the size of slow features imaged in the model. Not shown is a map of formal model uncertainty (computed using a Monte-Carlo technique) which is typically an order of magnitude smaller than the size of the slow anomalies imaged here. Fig. 2 does indeed indicate that structure in the lowermost mantle under the southern Indian Ocean is poorly resolved though resolution in the Pacific is adequate. In particular, resolution improves substantially as we move up in the mantle (due principally to the large number of crossing SS legs). This improvement in resolution is coincident with the Pacific plume region being imaged as several separate regions.

In regions of poor coverage, the first-difference smoothing incorporated in the inversion (see Masters et al., 2000) tends to result in laterally smeared structure with correspondingly lowered amplitude. In fact, the lowermost layer checkerboard test results in only about 50% amplitude recovery. We therefore strongly suspect that the southern hemisphere of the lowermost layer in our S velocity model is too small in amplitude and too smooth. Further improvements in data coverage (for example, by including diffracted phases) may well result in a rougher structure (more similar to the layers above) and with a larger amplitude.

Fig. 3 shows a 3D Cartesian representation of the Pacific superplume as viewed from the southwest. The isovelocity surface encloses velocity perturbations which are 1.1% slow or slower. This figure already shows some similarities to the numerical results of Fig. 9 which will likely be enhanced as resolution improves.

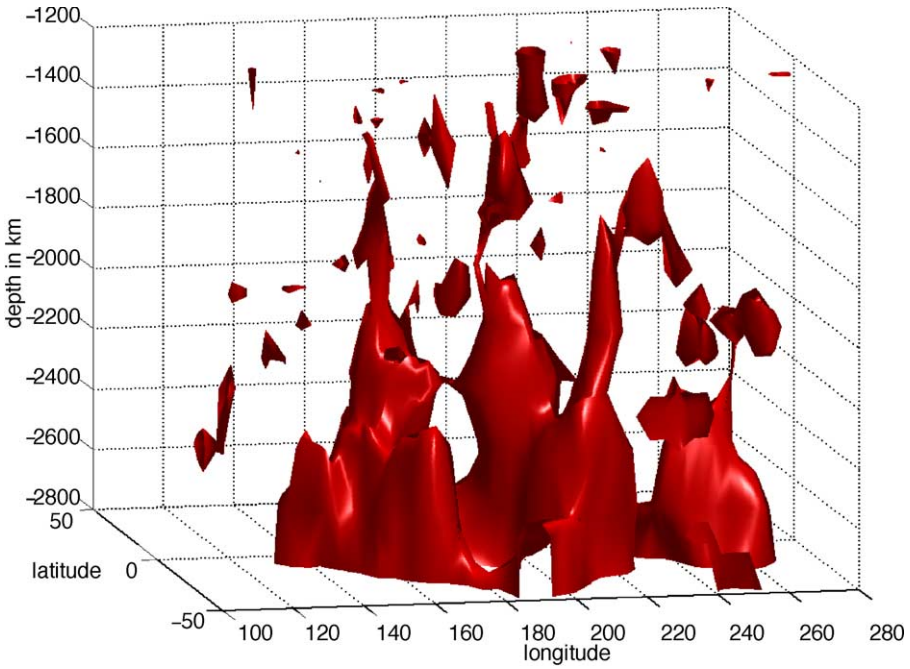

Fig. 3. Isovelocity surfaces (encompassing negative perturbations of 1.1% or more) of the Pacific superplume.

3. Mantle plumes

Before describing a superplume we should be clear about what we mean by a plume. We have yet to achieve an unambiguous detection of a mantle plume (cf., Rhodes and Davies, 2001), so our description of a plume is based on a theoretical picture of one (see, e.g., Schubert et al., 2001, for a discussion of mantle plumes).

A mantle plume is a buoyant upwelling which, if thermal in origin, results from the instability of a hot thermal boundary layer. A plume has a head and a tail or trailing conduit of rapidly, upwardly flowing, low viscosity, light or hot material. Plume heads may be hundreds to a thousand kilometers across and plume tails may be tens to a hundred kilometers in diameter. This head and tail structure is confirmed by various 2D and 3D numerical convection models, Malevsky and Yuen (1993) and Olson et al. (1993). A cluster of plume tails originating from a hot thermal boundary layer is seen in the results of the numerical convection model shown in Fig. 9.

There is some experimental evidence that not all thermal upwellings have this structure, however. For example, laboratory experiments by Jellinek et al. (2002) showed upwellings in the form of isolated thermals with parabolic-shaped heads and no distinguishable tails, such as occur in Rayleigh–Taylor instabilities. Isolated thermals are known to occur in situations where the instability depletes the thermal boundary layer, leaving no material for the conduit. The pervasiveness of the D''-layer argues that material is available there to feed mantle plume conduits. In addition, the longevity of certain hotspots, such as the Hawaiian chain, is hard to reconcile with a plume source consisting of a single thermal.

Plume buoyancy could be compositional as well as thermal in origin. Presumably then a superplume is an oversized version of a plume, with a head thousands to ten thousand kilometers across and a tail that is comparably large. Can such a structure exist? How does it form? Can a boundary layer not more than about a 100 km thick spawn a superplume?

4. Boundary layer instability

Considerations of thermal boundary layer stability and plume growth argue against the formation of superplumes from hot thermal boundary layers and for the formation of ordinary plumes with the dimensions quoted above. Instability of a hot thermal boundary layer leading to mantle plume formation has been extensively investigated using both numerical models and laboratory experiments (for example, Whitehead and Luther, 1975; Griffiths, 1986; Olson et al., 1987; Griffiths and Campbell, 1990; Malevsky and Yuen, 1993; Bercovici and Kelly, 1997; Farnetani, 1997; Kellogg, 1997; van Keken, 1997; Davaille et al., 2002; Jellinek and Manga, 2002). The following simplified picture, taken by Schubert et al. (2001) is derived from the results of these studies.

The instability occurs when the boundary layer Rayleigh number Ra_δ exceeds the critical value of the Rayleigh number Ra_{cr}. This happens after enough time t_{cr} has elapsed for the boundary layer to thicken and attain a critical width. The timescale t_{cr} is given by

$$t_{cr} = \frac{1}{\pi\kappa^{1/3}}\left(\frac{\nu Ra_{cr}}{\alpha g \Delta T}\right)^{2/3} \quad (1)$$

where κ is the thermal diffusivity, ν the kinematic viscosity, α the thermal expansivity, g the gravity, and ΔT the temperature drop cross the boundary layer. We assume values appropriate for the hot thermal boundary layer at the base of the lower mantle, $\kappa = 1 \times 10^{-6}\,\mathrm{m^2\,s^{-1}}$, $Ra_{cr} = 1.1 \times 10^3$ (appropriate for a layer with one rigid and one stress-free boundary), $\alpha = 1 \times 10^{-5}\,\mathrm{K^{-1}}$, $g = 10.5\,\mathrm{m\,s^{-2}}$. We consider two cases. The first is a large temperature increase across a low viscosity D''-layer, i.e., $\nu = 10^{20}\,\mathrm{Pa\,s}/5500\,\mathrm{kg\,m^{-3}}$ and $\Delta T = 1000\,\mathrm{K}$. This gives t_{cr} about 33 Myr. The corresponding critical boundary layer thickness $\delta_{cr} = (\pi\kappa t_{cr})^{1/2}$ is about 57 km. The second case assumes a small temperature increase across a high viscosity D''-layer, i.e., $\nu = 10^{21}\,\mathrm{Pa\,s}/5500\,\mathrm{kg\,m^{-3}}$ and $\Delta T = 200\,\mathrm{K}$. This gives t_{cr} about 450 Myr. The critical boundary layer thickness for this case is about 124 km. Thus, the tendency toward instability is heightened by low viscosity, a consequence of the high temperatures in the boundary layer and the strong temperature dependence of mantle viscosity. With low viscosity the hot thermal boundary layer at the CMB does not require much time to reach instability, and is comparatively thin when instability occurs. Even in the high viscosity case, the boundary layer thickness at instability is much less than superplume dimensions, although the instability is slow to develop.

Rayleigh–Taylor instability theory predicts that the spacing of incipient diapirs formed from the instability of the hot boundary layer at the base of the lower mantle is $\delta_{cr}(\nu_m/\nu_p)^{1/3}$, where ν_p is the kinematic viscosity of the hot boundary layer material forming the diapir and ν_m is the kinematic viscosity of the mantle just above the boundary layer. This is also the spacing of diapirs at separation. With $\nu_m/\nu_p = 10^2$ (the first case discussed above), this spacing is about 265 km. For the second case, $\nu_m/\nu_p = 10^1$, and the predicted spacing is 267 km, about the same. In Rayleigh–Taylor instability of a hot thermal boundary layer with temperature-dependent viscosity, the viscosity and temperature effects on the diapir spacing tend to offset each other. Incipient diapirs are only about 100 km across and are separated by only hundreds of kilometers.

An alternative way to model plume head formation considers the separation of a diapir from a boundary layer, and equates the speed of buoyant ascent of the diapir (given by the Stokes velocity for a spherical diapir) to its growth rate. This model gives

$$R_s = \left(\frac{3\nu_m Q_v}{4\pi g'}\right)^{1/4} \quad (2)$$

$$t_s = \left(\frac{4\pi}{3Q_v}\right)^{1/4}\left(\frac{\nu_m}{g'}\right)^{3/4} \quad (3)$$

where R_s is the radius at diapir separation, t_s the time required for the diapir to grow to that size, Q_v the volumetric rate at which the boundary layer supplies material to the diapir, and $g' = g(\rho_m - \rho_p)/\rho_m$ (ρ_p is the density of the diapir and ρ_m the density of the overlying mantle). With $Q_v = 13.7\,\mathrm{km^3}$ per year (the volumetric flux for the Hawaiian plume) and $\nu_m = 1.8 \times 10^{18}\,\mathrm{Pa\,s}$, Eqs. (2) and (3) give $R_s \cong 208\,\mathrm{km}$ and $t_s \cong 2.75\,\mathrm{Myr}$ for $g' = 0.1\,\mathrm{m\,s^{-2}}$, or $R_s \cong 311\,\mathrm{km}$ and $t_s \cong 9.2\,\mathrm{Myr}$ for $g' = 0.02\,\mathrm{m\,s^{-2}}$.

The time required for diapir separation from the boundary layer is generally shorter than the time required for the initial instability to develop. The entire

process of plume formation can occur in the hot lower mantle boundary layer within 50 Myr, and within 450 Myr if the layer is less heated. Bercovici and Kelly (1997) account for the local deflation of the boundary layer by the inflation of the growing diapir and obtain a somewhat different expression for R_s (namely, $R_s \cong \delta_{cr}(\nu_m/\nu_p)^{2/9}$) which gives $R_s = 160$ and 210 km for the two D''-layer viscosities considered above. These are only slightly smaller than the estimates gotten from the previous model, and well within the uncertainties of either method. The main point of all the above estimates of plume sizes and separations is that superplumes cannot originate from the instability of a hot thermal boundary layer at the base of the lower mantle. Superplumes are simply too large to have formed in this way. Either the so-called superplume regions of the lower mantle have a different origin, in which case they should probably be referred to differently, or the instability of the boundary layer must be suppressed, allowing the boundary layer to thicken toward superplume dimensions. If the boundary layer at the base of the mantle (the D''-layer) is both compositional and thermal, chemical composition might stabilize it. However, plume dimensions basically reflect the boundary layer thickness and the D''-layer is not more than a few hundred kilometers thick. Other ways to suppress boundary layer instability or promote diapir growth will be discussed below.

An alternative picture of the lower mantle superplume regions is suggested by the considerations of this section. These regions may be sites of groups or clusters of large numbers of "normal" plumes and seismic resolution is simply inadequate to discern this structure. The plume heads of large numbers of individual plumes would tend to grow and merge into a broad region of hot upwelling material as the plumes ascended through the mantle. Should a region formed in this way be referred to as a superplume? Probably not, because the dynamical implications of the term plume, described briefly above, would not pertain to a structure formed this way.

5. Mechanisms for the suppression of boundary layer instability and plume ascent

If boundary layer instability can be suppressed, then a lot of hot material in the boundary layer would have to pile-up before a buoyant upwelling could form. There are a number of mechanisms that can be thought of to accomplish this end. Among them are the effects of: (1) an endothermic phase transition in the deep lower mantle; (2) compositional gradients in a thermo-chemical boundary layer at the base of the lower mantle; (3) a viscosity maximum in the lower mantle; (4) a reduction in thermal expansivity or thermal conductivity in the lower mantle.

On Mars, the endothermic spinel to perovskite and magnesiowüstite phase change might occur just above the CMB. This phase change inhibits the ascent of hot upwellings until enough buoyant material accumulates to penetrate the transition (Schubert et al., 2001). The possible occurrence of this phase change just above the CMB has been hypothesized to explain the Tharsis superplume (Weinstein, 1995; Harder and Christensen, 1996; Harder, 1998, 2000). While this may work for Mars, there is no known endothermic phase change in the Earth's lower mantle.

The existence of a stabilizing chemical compositional gradient in the mantle boundary layer at the CMB (Montague et al., 1998) would allow the boundary layer to be thicker than a purely thermal boundary layer, but as noted above, the D''-layer in the mantle is not thick enough to launch a superplume, whatever its thermo-chemical nature. An endmember version of this effect is the model proposed by Kellogg et al. (1999), van der Hilst and Kárason (1999) and Montague and Kellogg (2000) in which a compositionally distinct thick (O, 10^3 km) and isolated layer resides at the bottom of the mantle. The lower thermal boundary layer in this model occurs along an undulating surface in the deep lower mantle. But this boundary layer is as unstable as a thermal boundary layer at the CMB; the source of "normal" plumes is simply displaced upwards from the CMB in this model. The pile-up of chemically heavy material at the base of the lower mantle by large-scale circulation could serve to focus the upwelling above the thickest piles of heavy material. Such upwellings could be large-scale if they are passive, i.e., controlled by the large-scale circulation in the lower mantle. However if they are active, i.e., positively buoyant and low viscosity, then our previous dynamical arguments for breakup into smaller scale plumes should apply to them also.

Any change in a thermal property like thermal expansivity or thermal conductivity that reduces the

buoyancy of hot material in the lower mantle will lead to larger buoyant structures. Uncertainties in these thermal properties, however, make it difficult to quantify their effects.

If there is a viscosity maximum in the lower mantle (van Keken and Yuen, 1995; Forte and Mitrovica, 2001), then rising diapirs must inflate by the addition of more light material so their additional buoyancy can overcome the increase in viscous resistance they experience in traversing a region of increasing viscosity. We evaluate this effect in the next section and show that any plausible lower mantle viscosity maximum is unable to account for a diapir with superplume dimensions.

5.1. Diapir rise through a region of upwardly increasing viscosity

We use a simple model to evaluate how a diapir will evolve as it rises through a region in which viscosity increases upwards. This simulates what happens to a diapir originating at the CMB and ascending toward the peak of a lower mantle viscosity maximum. The model assumes that a spherical plume head of radius R rises with the local Stokes velocity u_s. A trailing conduit is assumed to supply the plume head with buoyant material at the constant rate Q_v. The conduit lengthens at the rate at which the plume head is rising. Within the circular conduit of area A, flow is taken to be a laminar, parabolic, buoyantly driven Poiseuille flow. Mantle kinematic viscosity ν_m increases exponentially with height z above the CMB. This is an extension of the model developed by Whitehead and Luther (1975) for the steady rise of a diapir in a mantle with constant kinematic viscosity. In that case, it is straightforward to show

$$Q_v = AU_\infty \tag{4}$$

$$A = \left(\frac{8\pi\nu_p Q_v}{g'}\right)^{1/2} \tag{5}$$

$$U_\infty = \left(\frac{g' Q_v}{8\pi\nu_p}\right)^{1/2} \tag{6}$$

$$V_\infty = \frac{4\pi}{3}(3\nu_m)^{3/2}\left(\frac{Q_v}{8\pi g'\nu_p}\right)^{3/4} \tag{7}$$

where U_∞ is the upward velocity of the plume head, ν_p and g' are as defined previously, and V_∞ is the volume of the plume head. With $Q_v = 2.9\,\mathrm{km}^3$ per year (for the Reunion plume, Schubert et al., 2001) and other parameter values as above, one finds from Eqs. (4)–(7) that $U_\infty = 0.27$ m per year and $V_\infty = 2\times10^8\,\mathrm{km}^3$, corresponding to a plume radius of about 350 km and a conduit radius of about 60 km.

These are hardly the dimensions of a superplume (certainly the Reunion plume is not a superplume) so we return to the model of viscosity increasing with height above the CMB to see if that effect can substantially inflate the plume head. In this case, the plume head will grow as it rises at the rate

$$\frac{dV}{dt} = Q_v - Au_s \tag{8}$$

The local upward velocity of the plume head is given by the Stokes formula using the local kinematic viscosity of the mantle

$$u_s = \frac{g' R^2}{3\nu_m} \tag{9}$$

A is still given in Eq. (5) and ν_m is given by

$$\nu_m = \nu_{m_0}\, e^{z/H} \tag{10}$$

where ν_{m_0} is the kinematic viscosity of the mantle just above the CMB boundary layer and H is the length scale for the viscosity increase. Eqs. (5) and (8)–(10) can be combined and rewritten as

$$\frac{dF}{d\zeta} = \left\{e^{\lambda\zeta} - \left(\frac{2\gamma}{3}\right)^{1/2} F\right\} 2F^{-3/2} \tag{11}$$

where

$$\zeta = \frac{z}{R(0)} = z\left(\frac{3\nu_{m_0} Q_v}{4\pi g'}\right)^{-1/4} \tag{12}$$

$$F = \left(\frac{R}{R(0)}\right)^2 = R^2\left(\frac{3\nu_{m_0} Q_v}{4\pi g'}\right)^{-1/2} \tag{13}$$

$$\gamma = \frac{\nu_p}{\nu_{m_0}} \tag{14}$$

$$\gamma = \frac{R(0)}{H} \tag{15}$$

and $R(0)$ is the initial radius of the diapir. Eq. (11) is integrated with the boundary condition $F(0) = 1$. The square root of F gives the normalized radius of the

plume head and the upward speed of the plume head is given by

$$\frac{u_s}{u_s(0)} = F\left(\frac{\nu_m}{\nu_{m_0}}\right)^{-1} = F\,e^{-\lambda\zeta} \tag{16}$$

The way in which the plume head rises through the background viscosity increase, i.e., the solution of Eq. (11) subject to $F(0) = 1$ depends only on the two parameters λ, the ratio of the initial plume head radius to the viscosity length scale, and γ, the initial ratio of the viscosity of the plume material to the viscosity of the surrounding mantle.

Figs. 4 and 5 show the normalized radius of the plume head and the normalized plume speed as a function of the normalized distance above the CMB for $\gamma = 0.1$ (plume viscosity one-tenth the mantle viscosity just above the boundary layer) and $\lambda = 0.6908$, 0.4605, and 0.2303. For $\lambda = 0.6908$, mantle viscosity increases by 10^3 when the plume head has traveled upward a distance of 10 times its initial radius. For $\lambda = 0.4605$, the viscosity increase is 10^2 and for $\lambda = 0.2303$ it is 10. According to Fig. 5, the radius of the plume head increases monotonically with distance above the CMB, but only by factors of at most 2–6 even when the plume has traveled upward more than 10 times its initial radius through a viscosity stratification of factors of 10 to 10^3. The upward speed of the plume head shown in Fig. 5 first increases as the plume rises above the CMB, but the plume speed soon reaches a maximum after the plume has traversed about 1 or 2 times its initial radius. The plume head then slows down as it moves upward into regions of increasingly larger viscosity. The plume head never moves upward much faster than its initial speed and it slows down considerably when it encounters large viscosities.

In the limit $\gamma \to 0$, small plume viscosity compared with mantle viscosity, and $\lambda\zeta = z/H \gg 1$, many mantle viscosity scale heights above the CMB, Eq. (11) has an analytic solution given by

$$\frac{R}{R(0)} \sim \left(\frac{5\nu_m}{\lambda\nu_{m_0}}\right)^{1/5} \tag{17}$$

$$\frac{u_s}{u_s(0)} \sim \left(\frac{5}{\lambda}\right)^{2/5}\left(\frac{\nu_m}{\nu_{m_0}}\right)^{-3/5} \tag{18}$$

Eq. (17) shows that as the plume head moves upwards its radius increases asymptotically at the slow rate of

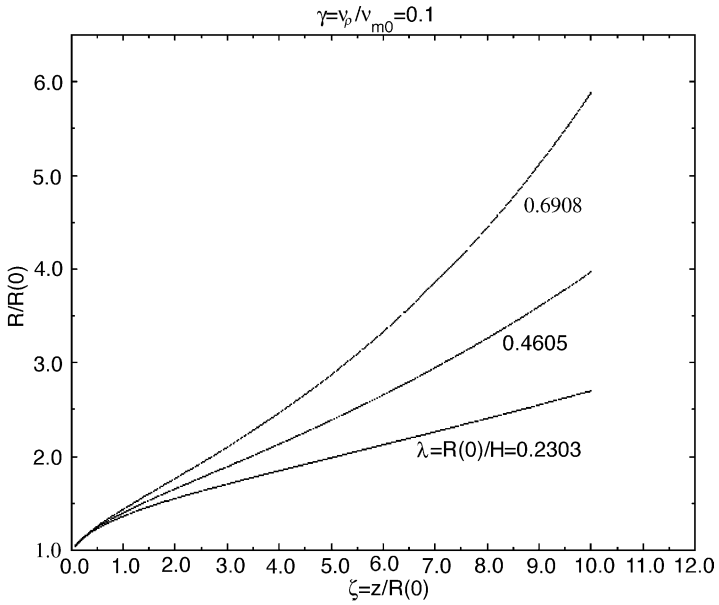

Fig. 4. Normalized radius of a plume head vs. normalized distance above the CMB for a plume rising through a background viscosity that increases exponentially with normalized distance above the CMB. The parameter λ is the inverse of the normalized scale height for the viscosity increase. The parameter γ is the ratio of plume viscosity to the viscosity of the mantle at the CMB.

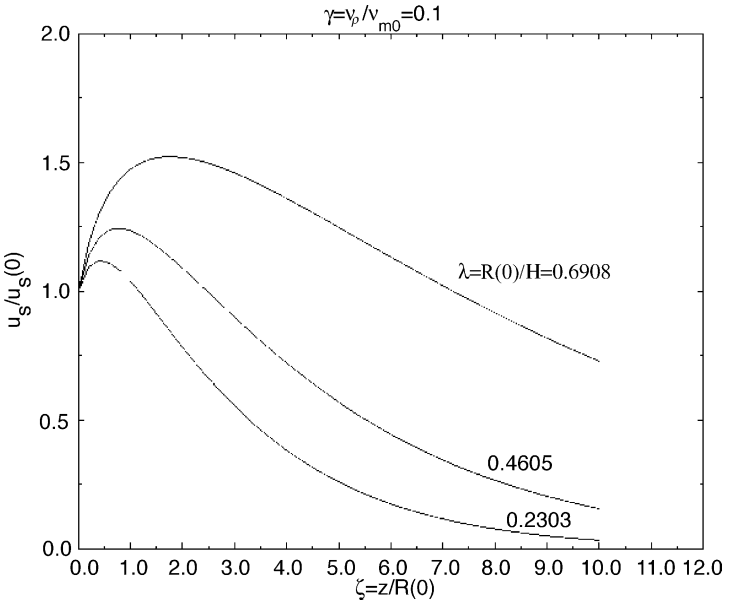

Fig. 5. Similar to Fig. 4 for the normalized rise speed of the plume head.

the mantle viscosity to the one-fifth power. Eq. (18) shows that the upward speed of the plume decreases more rapidly, with the inverse three-fifths power of the mantle viscosity.

The main conclusion of this analysis is that while a plume would increase in size as it moved upward toward a lower mantle viscosity maximum, the plume would still remain far smaller than the size of a superplume.

6. Plume clustering

The analysis in the previous section indicates that individual mantle plumes, originating as boundary layer instabilities in the D''-layer, are likely to be much smaller in size than the broad, seismically slow regions of the lower mantle below Africa and the south-central Pacific. Here we suggest an alternative interpretation for these two regions that is more consistent with the dynamical behavior of plumes as seen in laboratory and numerical models. We propose that these two regions contain clusters of smaller-scale plumes, instead of a single large-scale superplume as sketched in Fig. 6. A dense cluster of smaller plumes would appear as a region with lower than average seismic velocity in a low-resolution tomographic model of the mantle; the individual plumes that form the cluster would appear only at higher seismic resolution, as discussed later in this paper.

Plume clusters are a common phenomenon in high Rayleigh number convection (Manga and Weeraratne, 1999), especially in time-dependent convection with variable viscosity (Davaille and Jaupart, 1993). Clusters of plumes often form above variable boundary topography or variable boundary heat flow (Namiki and Kurita, 2001), and above piles of compositionally dense material (Olson and Kincaid, 1991; Tackley, 1998; Montague and Kellogg, 2000; Davaille et al., 2002; Jellinek and Manga, 2002). All of these are plausible situations in the lower mantle. In addition, plume clusters can occur without any contribution from boundary heterogeneity, through the action of larger-scale, externally driven flows, or by plume entrainment.

6.1. Plume concentration by external flows

It is well established that boundary layer instabilities and plumes are concentrated by externally imposed larger-scale flows. Both laboratory experiments (Kincaid et al., 1996; Jellinek et al., 2003) and

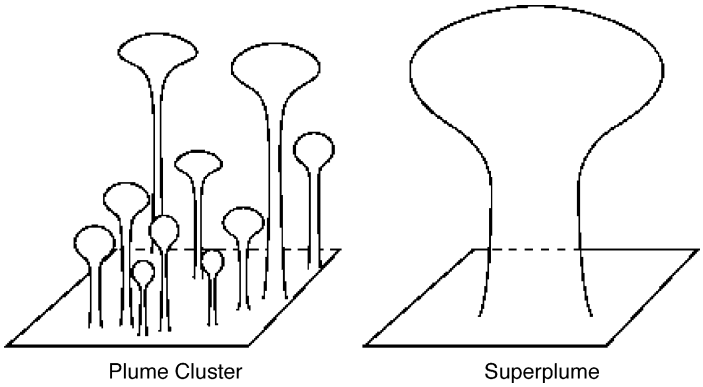

Fig. 6. Sketch of a plume cluster and a superplume.

numerical models (Rabinowicz et al., 1993; Ito et al., 1996) have demonstrated how plumes are focused by large-scale upwellings. There is abundant geophysical evidence that mantle plume concentrations are affected by large-scale motions in the mantle, including the low hotspot concentration near trenches and the high hotspot concentration near ridges (Weinstein and Olson, 1989), relative motion of hotspot tracks on different plates (Steinberger and O'Connell, 1998), along-strike variations in mid-ocean ridge structure (Parmentier and Morgan, 1990; Abelson and Agnon, 2001) and geochemical variations along ridges and at nearby hotspots (Schilling, 1985; Peate et al., 2001).

The numerical and laboratory studies of plume-ridge interaction show that the concentration of plumes beneath a divergent upper boundary depends on the ratio u_s/u_m, where u_s is the rise velocity of the plume (given here as the Stokes velocity of the plume head, according to Eq. (9)) and u_m is the characteristic velocity in the mantle induced by plate motions and subduction. For large values of this ratio, the background mantle circulation has little effect on the plumes. In the other extreme, when this ratio is very small, plume formation is suppressed and boundary layer instabilities are swept directly into the upwelling. For intermediate values of this ratio, which is the relevant regime for the mantle, the plumes are advected toward the upwelling by the large-scale flow, but their own upward motion prevents them from becoming fully captured. The result is anomalously high concentration of plumes ascending in the neighborhood of the large-scale upwelling, and conversely, anomalously low plume concentration near the downwellings, as seen in the experiments by Kincaid et al. (1996) and Jellinek et al. (2003).

There is geophysical evidence that plume concentration by global-scale flow may be important beneath both Africa and the south-central Pacific. The anomalously high surface topography above each of these regions is consistent with large-scale upward mantle flows there (Forte and Mitrovica, 2001). In addition, the density of hotspots is higher above these regions than the global average (Weinstein and Olson, 1989), even though many of these hotspots, particularly those above the African low-velocity structure, are small in magnitude (Sleep, 1990).

6.2. Plume concentration by entrainment

Plume clusters can also occur through the tendency of isolated groups of plumes to self-organize. The circulation induced by a rising plume includes a strong, inward-directed horizontal flow, sometimes referred to as the "entrainment wind". The entrainment wind induced by a single vertical plume conduit in a viscous fluid above a free-slip boundary (such as the core-mantle boundary) is symmetric about the conduit axis, and varies slowly with height above the boundary and with distance from the conduit. Neglecting these slow spatial variations, the (inward) entrainment wind velocity u_e near the base of a semi-infinite vertical plume conduit is (Olson et al., 1993)

$$u_e = \frac{g' r^2}{4\nu_m} \tag{19}$$

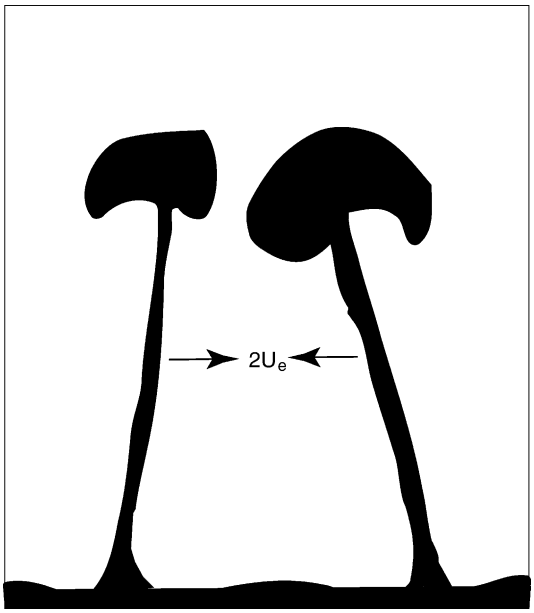

Fig. 7. Sketch showing the mutual entrainment of two isolated plumes.

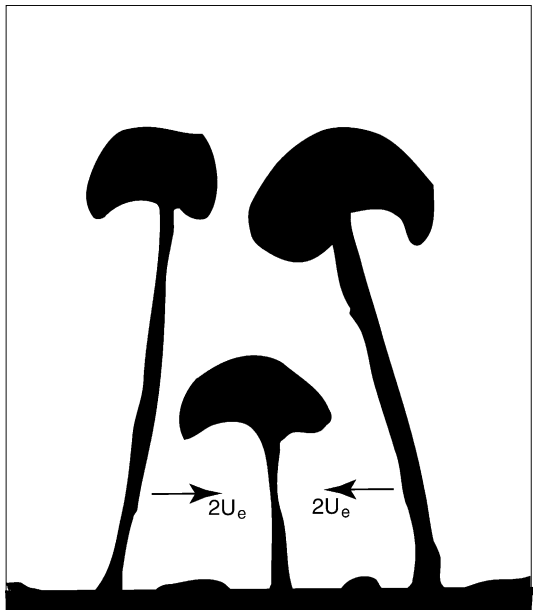

Fig. 8. Sketch showing the mutual entrainment of three isolated plumes.

where g' is the buoyancy of fluid in the plume conduit, r the conduit radius, and ν_m the viscosity of the external fluid, in this case the lower mantle.

Since the entrainment wind decreases slowly with distance, it tends to draw isolated plumes together, even if the plumes originate some distance apart. For example, the approach velocity of the two equal-sized plumes shown in Fig. 7 is $2u_e = g'r^2/2\nu_m$. Using the lower mantle and plume parameters from the previous section ($g' = 0.1\,\mathrm{m\,s^{-2}}$ and $\nu_m = 1 \times 10^{30}\,\mathrm{m^2\,s^{-1}}$) with $r = 120\,\mathrm{km}$, Eq. (19) gives an approach velocity of $2u_e = 1.2\,\mathrm{cm}$ per year, comparable to the rise velocity of small plumes in the lower mantle.

The entrainment wind causes pairs of isolated plumes to bend toward each other, as shown schematically in Fig. 7. This effect is often seen in two-dimensional numerical models of mantle convection (Vincent and Yuen, 1989; Balachandar et al., 1993; Balachandar and Yuen, 1994; Hansen and Yuen, 2000; Schubert et al., 2001). Entrainment is nearly as strong between the three co-linear plumes shown in Fig. 8. In this case the central plume is hardly affected, but each of the two edge plumes are attracted toward the central one with entrainment velocity nearly $2u_e$. Entrainment winds also affect two-dimensional configurations of isolated plumes. For example, each of the four equal plumes located at the corners of a square are attracted toward the center with velocity $(1 + \sqrt{2})u_e$. We note that plumes in the interior of large clusters are not affected in the same way as the plumes on the edge of the cluster, since the entrainment wind is nearly zero in the cluster interior. This explains why large plume clusters (or large arrays of plumes) do not often condense into a single superplume.

Another type of entrainment that contributes to plume clustering is the interaction of plume heads. The flow field around a plume head is dipolar, with flow towards the plume head from below. Thus, the smaller plume heads emerging from a thermal boundary layer after a larger plume tend to get drawn into the larger plume from below.

6.3. 3D numerical simulation

The physical mechanisms of plume clustering discussed above are apparent in the 3D numerical calculation shown in Fig. 9. The plume clusters shown in the figure arise from a model with a rheology and other physical properties thought to be realistic for

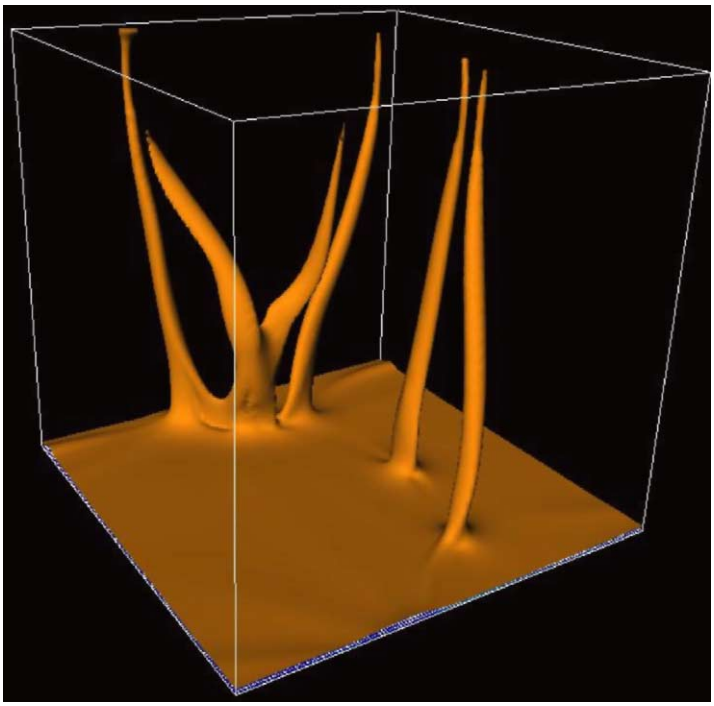

Fig. 9. Plume clusters in a 3D numerical model. Details of the model are given in the text.

Earth's lower mantle. The basic compressible, anelastic model with depth-dependent thermal expansivity, conductivity, and reference density is similar to that described by Tackley (2002). The rheology is based on a homologous law

$$\eta(T,z) = \bar{A}\exp\left(\bar{g}\frac{T_{\mathrm{m}}(z)}{T}\right) \tag{20}$$

with $\bar{g} = 13.5$, a reasonable value for the lower mantle (Yamazaki and Karato, 2001). The melting temperature $T_{\mathrm{m}}(z)$ in the model (z is the vertical coordinate) is based on simple fits to the experimental solidii of Zerr et al. (1998) in the lower mantle and Herzberg et al. (2000) in the upper mantle. The constant factor $\bar{A}$ is set such that the viscosity for an adiabat with a potential temperature of 1600 K is 10^{22} Pa s at the core-mantle boundary (CMB). The model is configured to study plumes, with the top of the domain representing the base of a rigid, isothermal lithosphere with a temperature of 1600 K, and the base of the model representing a free-slip, isothermal CMB with a temperature of 3712 K, giving a superadiabatic temperature rise of 1200 K, all of which occurs over the lower boundary layer. The initial condition for temperature is a 1600 K adiabat with an error-function thermal boundary layer at the CMB with thickness 70 km and random perturbations of peak-to-peak amplitude 60 K. In order to prevent the build-up of hot material in the upper part of the domain, temperature deviations from the 1600 K adiabat are damped out in the upper 10% of the box.

The calculation is performed using the code Stag3D (Tackley, 1996, 2002), but with a new advection scheme based on upstream tracking and interpolation, similar to characteristics-based methods (Malevsky and Yuen, 1991), thereby minimizing numerical diffusion and overshoot. A $128 \times 128 \times 128$ grid is utilized, with vertical grid refinement near the CMB. With the above parameters and this grid spacing, tens of thousands of timesteps are necessary to calculate relatively short geological times (e.g., 100 million years).

The system initially undergoes a transient, in which the lower boundary layer thickens and develops

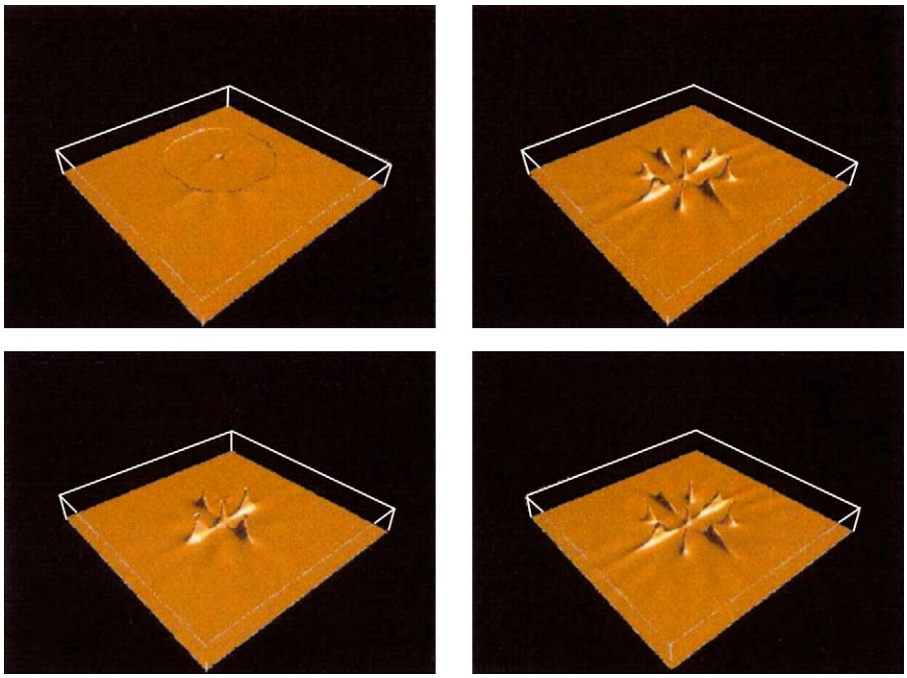

Fig. 10. The decay of a superplume into a cluster of nine plumes. In the initial state (upper left), a superplume is produced by the strong increase of viscosity with pressure. Upon the addition of temperature dependence of the viscosity, the superplume breaks up with time (lower left to upper right to lower right) into the cluster of nine smaller plumes shown in the lower right. From a numerical calculation by Hansen and Yuen (2002).

multiple small-scale instabilities that are swept into two large-scale instabilities. Then it settles down into two slowly evolving plume conduits, which are subsequently added to by three starting plumes, forming a plume cluster. The illustrated time is about 100 million years.

Hansen and Yuen (2002) have carried out another calculation that illustrates the development of a plume cluster from an initial state of large-scale upwelling that could be described as a superplume. Fig. 10, from their calculation, shows the breakup of a superplume (top left) into a plume cluster (bottom right). The initial superplume state results from a viscosity that depends only on pressure or depth; viscosity increases strongly with depth as depth to the fifth power. The surface Rayleigh number was 10^7, and thermal expansivity decreased by a factor of 3 with depth. Upon the addition of an exponential dependence of viscosity on temperature (viscosity varies by 10^3 due to temperature) the superplume decays into a cluster of nine smaller plumes. The preferred state for the more realistic viscosity dependence on both temperature and pressure is a plume cluster, not a superplume.

7. Summary

We have studied the possibility that the broad, seismically slow structures beneath Africa and the south-central Pacific are really under-resolved plume clusters instead of superplumes. A mantle plume is a buoyant upwelling that forms from the instability of a hot thermal (or thermo-chemical) boundary layer at the base of the mantle (Schubert et al., 2001). We reviewed the dynamics of boundary layer instability and showed that the thermal boundary layer at the base of the mantle gives rise to plumes that are only O (100 km) across. Superplume regions are too large to be explained by a single instability of the D''-layer. Instead, if such broad, hot, upwelling regions of the

mantle have their origin in the instability of a boundary layer at the CMB, then the regions must contain a large number of ordinary plumes, i.e., they must be plume forests or clusters.

Clusters of plumes are formed by the dynamics of large-scale flows. Horizontal convergence toward large-scale upwelling sweeps plumes into groups. Entrainment by plume-induced flow also promotes the formation of clusters. We presented a new numerical 3D calculation that exemplifies these dynamical effects. The locations of hotspots in relation to oceanic ridges supports the concentration of plumes by large-scale upwelling in the mantle. The likelihood of large-scale upwelling beneath Africa and the south-central Pacific favors the accumulation of plumes in these regions. Johnson and Richards (2003) have proposed that the distribution of coronae on Venus can be understood if coronae are products of mantle plumes that are gathered into clusters by large-scale mantle upwelling.

We investigated whether the rise of a plume into increasingly more viscous mantle could broaden plume heads to superplume size. Upward motion of a plume head from the CMB toward a lower mantle viscosity maximum would increase the radius of a plume head, but not nearly enough to account for the size of a superplume.

In summary, all of these dynamical considerations indicate that buoyant plumes from the D''-layer tend to a characteristic size which is far smaller than the observed superplume regions. Of course, this still leaves open the possibility that the superplume regions represent passive upwellings in the large-scale circulation of the lower mantle that are nevertheless seismically identifiable. Such passive upwellings would not be subject to the same instabilities we have discussed here.

One way to determine if the superplumes beneath Africa and the south-central Pacific are really plume clusters is to seismically observe the small-scale structure characteristic of a cluster. We presented a new S-wave velocity model of the lower mantle that shows considerable structure near the CMB beneath the south-central Pacific; the Pacific superplume consists of at least six smaller-scale centers of reduced S-wave speed. The model also shows that the Africa superplume breaks up into at least two and perhaps three smaller-scale plumes. While seismic resolution is still inadequate to reveal all the small-scale structure of these regions, the break-up of these superplumes into concentrations of smaller plumes is a certainty.

Acknowledgements

We thank U. Hansen and D. Yuen for the opportunity to include their figure as Fig. 10 of this paper. GS acknowledges support from the NASA Planetary Geology and Geophysics Program under grant NAG 5-1161. GM acknowledges support from grant NSF EAR01-12289.

References

Abelson, M., Agnon, A., 2001. Hotspot activity and plume pulses recorded by geometry of spreading axes. Earth Planet. Sci. Lett. 189, 31–47.

Balachandar, S., Yuen, D.A., 1994. Three-dimensional fully spectral numerical method for mantle convection with depth-dependent properties. J. Comp. Phys. 113, 62–74.

Balachandar, S., Yuen, D.A., Reuteler, D., 1993. Viscous and adiabatic heating effects in three-dimensional compressible convection at infinite Prandtl number. Phys. Fluids A 5, 2938–2945.

Bercovici, D., Kelly, A., 1997. The non-linear initiation of diapirs and plume heads. Phys. Earth Planet. Int. 101, 119–130.

Davaille, A., Girard, F., Le Bars, M., 2002. How to anchor hotspots in a convecting mantle? Earth Planet. Sci. Lett. 203, 621–634.

Davaille, A., Jaupart, C., 1993. Transient high-Rayleigh-number thermal convection with large viscosity variations. J. Fluid Mech. 253, 141–166.

Farnetani, C.G., 1997. Excess temperature of mantle plumes: the role of chemical stratification across D''. Geophys. Res. Lett. 24, 1583–1586.

Forte, A.M., Mitrovica, J.X., 2001. Deep-mantle high-viscosity flow and thermochemical structure inferred from seismic and geodynamic data. Nature 410, 1049–1056.

Griffiths, R.W., 1986. Thermals in extremely viscous fluids, including the effects of temperature-dependent viscosity. J. Fluid Mech. 166, 115–138.

Griffiths, R.W., Campbell, I.H., 1990. Stirring and structure in mantle starting plumes. Earth Planet. Sci. Lett. 99, 66–78.

Hager, B.H., Clayton, R.W., Richards, M.A., Comer, R.P., Dziewonski, A.M., 1985. Lower mantle heterogeneity, dynamic topography and the geoid. Nature 313, 541–545.

Hansen, U., Yuen, D., 2002. Modelling constraints from boundary layer estimates on the sharpness of superplumes in the lower mantle. Eos Trans. AGU 83 (47), Fall Meeting Suppl., Abstract U72B-0031.

Hansen, U., Yuen, D.A., 2000. Extended-Boussinesq thermal-chemical convection with moving heat sources and variable viscosity. Earth Planet. Sci. Lett. 176, 401–411.

Harder, H., 1998. Phase transitions and the three-dimensional platform of thermal convection in the Martian mantle. J. Geophys. Res. 103, 16775–16797.

Harder, H., 2000. Mantle convection and the dynamic geoid of Mars. Geophys. Res. Lett. 27, 301–304.

Harder, H., Christensen, U.R., 1996. A one-plume model of Martian mantle convection. Nature 380, 507–509.

Herzberg, C., Raterron, P., Zhang, J., 2000. New experimental observations on the anhydrous solidus for peridotite KLB-1. Geochem. Geophys. Geosyst. 1, Pap. no. 2000GC000089.

Ito, G., Lin, J., Gable, C.W., 1996. Dynamics of mantle flow and melting at a ridge-centered hotspot: Iceland and the mid-Atlantic ridge. Earth Planet. Sci. Lett. 144, 53–74.

Jellinek, A.M., Gonnermann, H.M., Richards, M.A., 2003. Plume capture by divergent plate motions: implications for the distribution of hotspots, geochemistry of mid-ocean ridge basalts, and estimates of the heat flux at the core-mantle boundary. Earth Planet. Sci. Lett. 205, 361–378.

Jellinek, A.M., Lenardic, A., Manga, M., 2002. The influence of interior mantle temperature on the structure of plumes: heads for Venus, tails for the Earth. Geophys. Res. Lett. 29, 27-1. doi: 10.1029/2001GL014624.

Jellinek, A.M., Manga, M., 2002. The influence of a chemical boundary layer on the fixity, spacing and lifetime of mantle plumes. Nature 418, 760–763.

Johnson, C.L., Richards, M.A., 2003. A conceptual model for the relationship between coronae and large-scale mantle dynamics on Venus. J. Geophys. Res. 108, 5058. doi: 10.1029/2002JE001962.

Kellogg, L.H., 1997. Growing the Earth's D''-layer: effects of density variations at the core-mantle boundary. Geophys. Res. Lett. 24, 2749–2752.

Kellogg, L.H., Hager, B.H., van der Hilst, R.D., 1999. Compositional stratification in the deep mantle. Science 283, 1881–1884.

Kincaid, C., Sparks, D.W., Detrick, R., 1996. The relative importance of plate-driven and buoyancy-driven flow at mid-ocean ridges. J. Geophys. Res. 101, 16177–16193.

Malevsky, A.V., Yuen, D.A., 1991. Characteristics-based methods applied to infinite Prandtl number thermal-convection in the hard turbulent regime. Phys. Fluids 3, 2105–2115.

Malevsky, A.V., Yuen, D.A., 1993. Plume structures in the hard-turbulent regime of three-dimensional infinite Prandtl number convection. Geophys. Res. Lett. 20, 383–386.

Manga, M., Weeraratne, D., 1999. Experimental study of non-Boussinesq Rayleigh–Bénard convection at high Rayleigh and Prandtl numbers. Phys. Fluids 11, 2969–2976.

Masters, G., Johnson, S., Laske, G., Bolton, H., 1996. A shear velocity model of the mantle. Phil. Trans. Roy. Soc. Lond. 354A, 1385–1411.

Masters, G., Laske, G., Bolton, H., Dziewonski, A., 2000. The relative behavior of shear velocity, bulk sound speed, and compressional velocity in the mantle: implications for chemical and thermal structure. In: Karato, S., Forte, A.M., Liebermann, R.C., Masters, G., Stixrude, L. (Eds.), Earth's Deep Interior: Mineral Physics and Tomography, vol. 117 of AGU Monograph. American Geophysical Union, Washington, DC, pp. 63–87.

Mégnin, C., Romanowicz, B., 2000. The three-dimensional shear velocity structure of the mantle from the inversion of body, surface and higher-mode waveforms. Geophys. J. Int. 143, 709–728.

Montague, N.L., Kellogg, L.H., 2000. Numerical models of a dense layer at the base of the mantle and implications for the geodynamics of D''. J. Geophys. Res. 105, 11101–11114.

Montague, N.L., Kellogg, L.H., Manga, M., 1998. High Rayleigh number thermo-chemical models of a dense boundary layer in D''. Geophys. Res. Lett. 25, 2345–2348.

Namiki, A., Kurita, K., 2001. The influence of boundary heterogeneity in experimental models of mantle convection with internal heat sources. Phys. Earth Planet. Int. 128, 195–205.

Olson, P., Kincaid, C., 1991. Experiments on the interaction of thermal convection and compositional layering at the base of the mantle. J. Geophys. Res. 96, 4347–4354.

Olson, P., Schubert, G., Anderson, C., 1987. Plume formation in the D''-layer and the roughness of the core-mantle boundary. Nature 327, 409–413.

Olson, P., Schubert, G., Anderson, C., 1993. Structure of axisymmetric mantle plumes. J. Geophys. Res. 98, 6829–6844.

Parmentier, E.M., Morgan, J.P., 1990. Spreading rate dependence of three-dimensional structure in oceanic spreading centres. Nature 348, 325–328.

Peate, D.W., Hawkesworth, C.J., van Calsteren, P.W., Taylor, R.N., Murton, B.J., 2001. ^{238}U–^{230}Th constraints on mantle upwelling and plume-ridge interaction along the Reykjanes ridge. Earth Planet. Sci. Lett. 187, 259–272.

Rabinowicz, M., Rouzo, S., Sempere, J.-C., Rosemberg, C., 1993. Three-dimensional mantle flow beneath mid-ocean ridges. J. Geophys. Res. 98, 7851–7869.

Rhodes, M., Davies, J.H., 2001. Tomographic imaging of multiple mantle plumes in the uppermost lower mantle. Geophys. J. Int. 147, 88–92.

Ritsema, J., van Heijst, H.J., Woodhouse, J.H., 1999. Complex shear wave velocity structure imaged beneath Africa and Iceland. Science 286, 1925–1928.

Romanowicz, B., Gung, Y., 2002. Superplumes from the core-mantle boundary to the lithosphere: implications for heat flux. Science 296, 513–516.

Schilling, J.-G., 1985. Upper mantle heterogeneities and dynamics. Nature 314, 62–67.

Schubert, G., Turcotte, D.L., Olson, P., 2001. Mantle Convection in the Earth and Planets. Cambridge University Press, Cambridge, UK.

Sleep, N.H., 1990. Hotspots and mantle plumes: some phenomenology. J. Geophys. Res. 95, 6715–6736.

Steinberger, B., O'Connell, R.J., 1998. Advection of plumes in mantle flow: implications for hotspot motion, mantle viscosity and plume distribution. Geophys. J. Int. 132, 412–434.

Su, W., Woodward, R.L., Dziewonski, A.M., 1994. Degree 12 model of shear velocity heterogeneity in the mantle. J. Geophys. Res. 99, 6945–6980.

Tackley, P.J., 1996. Effects of strongly variable viscosity on three-dimensional compressible convection in planetary mantles. J. Geophys. Res. 101, 3311–3332.

Tackley, P.J., 1998. Three-dimensional simulations of mantle convection with a thermo-chemical basal boundary layer: D''? In: Gurnis, M., Wysession, M.E., Knittle, E., Buffett, B.A. (Eds.), The Core-Mantle Boundary Region, vol. 28 of Geodynamics Series. American Geophysical Union, Washington, DC, pp. 231–253.

Tackley, P.J., 2002. Strong heterogeneity caused by deep mantle layering. Geochem. Geophys. Geosyst. 3. doi: 10.1029/2001GC000167.

van der Hilst, R.D., Kárason, H., 1999. Compositional heterogeneity in the bottom 1000 km of Earth's mantle: toward a hybrid convection model. Science 283, 1885–1888.

van Keken, P., 1997. Evolution of starting mantle plumes: a comparison between numerical and laboratory models. Earth Planet. Sci. Lett. 148, 1–11.

van Keken, P.E., Yuen, D.A., 1995. Dynamical influences of high viscosity in the lower mantle induced by the steep melting curve of perovskite: effects of curvature and time dependence. J. Geophys. Res. 100, 15233–15248.

Vincent, A.P., Yuen, D.A., 1989. Multimode mean-field filtering experiments for chaotic thermal convection. Geophys. Astrophys. Fluid Dyn. 47, 131–156.

Weinstein, S.A., 1995. The effects of a deep mantle endothermic phase change on the structure of thermal convection in silicate planets. J. Geophys. Res. 100, 11719–11728.

Weinstein, S.A., Olson, P.L., 1989. The proximity of hotspots to convergent and divergent plate boundaries. Geophys. Res. Lett. 16, 433–436.

Whitehead, J.A., Luther, D.S., 1975. Dynamics of laboratory diapir and plume models. J. Geophys. Res. 80, 705–717.

Yamazaki, D., Karato, S., 2001. Some mineral physics constraints on the rheology and geothermal structure of Earth's lower mantle. Am. Mineral. 86, 385–391.

Zerr, A., Diegeler, A., Boehler, R., 1998. Solidus of Earth's deep mantle. Science 281, 243–246.